

Radiation from flexural vibrations of the baseplate and their effect on the accuracy of traveltime measurements

A. Lebedev* and I. Beresnev

Department of Geological and Atmospheric Sciences, Iowa State University, 253 Science 1, Ames, IA 50011-3212, USA

Received January 2004, revision accepted October 2004

ABSTRACT

We analyse the problem of radiation of seismic waves by a vibroseis source when the baseplate is subject to flexure. A theoretical model is proposed to account for baseplate flexure, generalizing the well-known model of the vibroseis source of Sallas and Weber, which was developed for a rigid plate. Using the model proposed, we analyse the effect of flexure on the properties of seismic waves. We show that the flexure does not contribute to the far-field and mainly affects the readings of the reference accelerometer that is used to measure the force applied to the ground; these readings generally become dependent on the location of the sensor on the plate. For muddy and sandy soils, the effect of flexure on baseplate-acceleration measurements is nonetheless pronounced at the high end of the vibroseis frequency band only (~ 100 Hz), and is negligible at all frequencies for stiffer soils. The corresponding phase lags introduced by the flexural vibrations at high frequencies lead to errors in the traveltime measurements (through the cross-correlation function) of up to 0.6 ms for muddy soils and less for denser soils. We show the existence of an optimal position of the reference sensor on the baseplate and also propose a general method of eliminating the phase lag due to the baseplate flexure in acceleration measurements.

INTRODUCTION

Vibroseis sources are the principal sources of seismic energy in land exploration. Seismic waves are excited by alternating the force applied to the ground. To obtain high-quality earth images, it is important to take the true radiated signal as the reference in calculating the cross-correlation function with the far-field waveform, instead of using the theoretical sweep. Such a true signal is the force applied to the ground. For example, knowing the exact radiated signal would enable us to account for resonant ground behaviour or non-linear contact effects, which represent the distortion of the theoretical pilot as it enters the ground.

The applied force can be determined as a ‘weighted sum’ of the accelerations of the baseplate and the reaction mass (Sallas and Weber 1982; Safar 1984; Sallas 1984; Baeten and

Ziolkowski 1990). In this case, one of the accelerometers should be placed directly on the baseplate. However, since the plate is subject to flexural vibrations, placing the reference accelerometer in different locations within the plate will generally produce different records. It is therefore important to understand how these differences in the estimated force signal, caused by plate flexure, will affect the cross-correlation with the far-field waveform. The investigation of this problem is the objective of our study.

THEORETICAL BACKGROUND

Model of the vibrator

The ground-reaction force (Fig. 1) can be determined from the measured accelerations of the reaction mass and the baseplate as (Sallas and Weber 1982; Sallas 1984)

$$-F_g = M_1 \ddot{z}_1 + M_2 \ddot{z}_2, \quad (1)$$

*E-mail: swan@hydro.appl.sci-iiit.ac.in

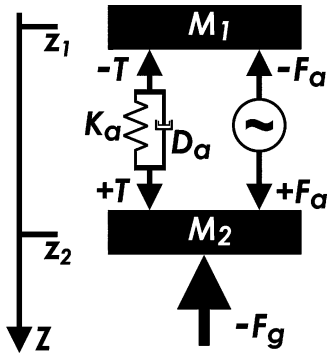


Figure 1 Equivalent lumped-parameter mechanical model of a seismic vibrator, corresponding to system (4). The forces F_a and T are shown applied at separate points for illustrative purposes only; realistically they are applied at the same point at the centre of the plate.

where M_1 and M_2 are the reaction mass and the mass of the baseplate, respectively, and \ddot{z}_1 and \ddot{z}_2 are the corresponding accelerations. Equation (1) provides the ground-reaction value for an inflexible baseplate, while the acceleration \ddot{z}_2 , realistically measured by a baseplate sensor, will be composed of two parts,

$$\ddot{z}_2 = \ddot{z}_2^{\text{whole}} + \ddot{z}_2^{\text{flexure}}, \quad (2)$$

where $\ddot{z}_2^{\text{whole}}$ corresponds to the movement of the baseplate ‘as a whole’ (uniform displacement) and $\ddot{z}_2^{\text{flexure}}$ is the added flexural-vibration term. It is known from structural acoustics (e.g. Junger and Feit 1986) that the flexural deformations of a plate with free boundaries are a very inefficient source of elastic-wave radiation when the wave size of the plate is small (see Appendix A). Consequently, due to the small size of the plate relative to the radiated wavelengths in the operating band of the vibroseis devices (e.g. Safar 1984), only the displacement as a whole will contribute significantly to the far-field response. The ground force F_g determined from (1) will thus include the non-zero terms that do not affect the far-field radiation. Note that it is impossible to isolate $\ddot{z}_2^{\text{whole}}$ from $\ddot{z}_2^{\text{flexure}}$ in real measurements, which only provide a composite value (2). The issue is thus to discover how close the realistically measured quantity \ddot{z}_2 is to $\ddot{z}_2^{\text{whole}}$; any differences between them will lead to an unknown distortion in the correlation function.

Theoretically, the measured value of \ddot{z}_2 can be made as close as necessary to $\ddot{z}_2^{\text{whole}}$ by placing the reference accelerometer at an appropriate point on the plate where $\ddot{z}_2^{\text{flexure}}$ is much smaller than $\ddot{z}_2^{\text{whole}}$. For example, any point on a nodal line of the flexural modes could be considered a good choice for

the measurement. However, there are two problems in finding such a location. Firstly, the nodal lines are not the same for all flexural modes. Secondly, these lines can be found easily in a theoretical approach but not in practice. Any deviation from the theoretical nodal position in the measurements would be undesirable due to its effect on the correlation function.

We model the baseplate deformations as the deformations of a circular plate with a force applied at the centre. The exact shape of the baseplate is not important as long as its size remains small relative to the wavelength. Since this condition is a good approximation in the operating bands of vibroseis devices, the conclusions of this analysis will apply equally to the realistic plate shapes. In this approximation, it is also possible to consider the vibroseis device as a vibratory system with lumped parameters. The ground force for the rigid (inflexible) baseplate is defined by Sallas (1984) in terms of the acceleration of the captured mass (M_g), the deformation of the captured spring (K_g), and the velocity of the dashpot (D_g) (describing losses due to radiation) as

$$F_g = M_g \ddot{z}_2 + D_g \dot{z}_2 + K_g z_2. \quad (3)$$

This force controls the radiated signals. The displacements in the ‘baseplate – reaction mass’ oscillatory system are described by the governing equations (Lerwill 1981; Sallas and Weber 1982; Sallas 1984),

$$\begin{aligned} M_1 \ddot{z}_1 &= -F_a(t) - T, \\ M_2 \ddot{z}_2 &= +F_a(t) + T - F_g, \\ T &= D_a(\dot{z}_1 - \dot{z}_2) + K_a(z_1 - z_2), \end{aligned} \quad (4)$$

where \dot{z}_1 , \dot{z}_2 and z_1 , z_2 are the velocity and the displacement time histories, respectively. The quantity T in (4) is the coupling force between the reaction mass and the baseplate. The element K_a is the spring constant for the airbag suspension of the reaction mass, and D_a is the dashpot constant for the airbag, accounting for the corresponding losses. The actuator force is F_a . The equivalent mechanical model for the lumped-parameter system (4) is shown in Fig. 1.

It will be assumed that the actuator force is sinusoidal with angular frequency ω , i.e. $F_a(t) = F_a \exp(-i\omega t)$, and that it is applied at the centre of the baseplate. We have introduced the quantity T for convenience, but it should be recalled that it is applied at the point of application of F_a , i.e. at the centre of the plate. The properties of a steel baseplate, as described by Safar (1984), are used throughout the paper, i.e. it has an area of 2.35 m² and a mass of 681 kg (Table 1).

Table 1 Soil and source parameters used in calculations (also see tables 2 and 3 of Safar 1984)

Parameter	Soil type		
	Mud	Sand	Chalk
Soil density (kg/m ³)	1500	2500	1800
P-wave velocity (m/s)	1400	488	2140
S-wave velocity (m/s)	90	244	1235
Captured mass M_g (kg)	1512	1236	773
Captured rigidity K_g (10 ⁷ N/m)	8.33	76.9	127
Captured dashpot D_g (10 ⁶ kg/s)	0.66	2.15	7
Reaction mass M_1 (kg)		1773	
Baseplate mass M_2 (kg)		681	
Spring constant K_a (10 ⁵ N/m)		6.25	
Dashpot constant D_a (kg/s)		10 000	
Density of baseplate ρ_s (steel) (kg/m ³)		7800	
Young modulus of baseplate E (GPa)		200	
Poisson's ratio of baseplate ν		0.3	
Baseplate radius R_0 (m)		0.865	
Baseplate thickness h calculated as $M_2/\rho_s\pi R_0^2$ (m)		0.037	

Accounting for baseplate flexure

Equations (3) and (4) are valid for the rigid baseplate. The flexural deformations can be accounted for by the superposition of natural modal responses to harmonic excitation (e.g. Morse and Feshbach 1953, chapter 6.3; Junger and Feit 1986, chapter 7.10), i.e.

$$z_2(\omega, r) = z_2^{\text{whole}}(\omega) + z_2^{\text{flexure}}(\omega, r) = \sum_{n=0}^{\infty} a_n(\omega) \psi_n(r), \quad 0 \leq r \leq R_0, \quad (5)$$

where $a_n(\omega)$ is the complex amplitude of the n th mode, the set of eigenfunctions $\psi_n(r)$ is the orthonormal basis describing the displacement at the radius r from the baseplate centre, and the radius of the baseplate is R_0 . The terms in (5) with $n > 0$ describe the baseplate flexure and give an explicit formulation of z_2^{flexure} introduced in (2), while the term with $n = 0$ is the uniform displacement z_2^{whole} . In (5), $z_2(\omega, r)$ is the amplitude of the baseplate displacement at a given excitation frequency ω ; the time history is obtained by multiplying it by the factor $\exp(-i\omega t)$. As (5) shows, we chose to decompose the displacement of the plate on the ground into a superposition of free-oscillation modes. Since these modes form an orthonormal basis, such decomposition is always possible. The exact form of the functions $\psi_n(r)$ is found as described in Appendix A.

To account for the additional flexural terms introduced in (5), equations (3) and (4) are generalized as follows. Equation (3) becomes

$$F_g(\omega, r) = -i\omega S \sum_{n=0}^{\infty} Z_n(\omega) a_n(\omega) \psi_n(r), \quad (6)$$

where Z_n is the radiation impedance (B5) per unit area, corresponding to the displacements distributed over the baseplate in the n th mode (see Appendix B), and $S = \pi R_0^2$ is the baseplate area. For the case of the rigid displacement ($n = 0$), we set

$$Z_0(\omega) S = -i\omega M_g + D_g + iK_g/\omega, \quad (7)$$

so that (6) is identical to (3), assuming $z_2^{\text{whole}}(\omega) = a_0(\omega)\psi_0(\omega)$.

The first equation in system (4) remains the same with the only difference that z_2 is now represented by (5). This gives equation (8a). The second equation in (4) must be replaced by a more general equation determining the modal amplitudes a_n . To this end, we substitute (5) in the equation of motion of the plate (A1) (see Appendix A), keeping in mind that the terms $\psi_n(r)$ satisfy (A1) when its right-hand side is zero. In accordance with the description in Appendix A, we include the force acting at the plate centre ($F_a + T$) and the ground-reaction force ($-F_g(\omega, r)$) defined by (6) in the right-hand side of (A1). Then the integration of both sides of (A1) over the plate area with weighting $\psi_n(r)$ and the orthogonality conditions (A3) leads to the equations for the modal amplitudes (8b):

$$-M_1\omega^2 z_1 = -F_a - T(\omega), \quad (8a)$$

$$[\rho_s h (-\omega^2 + \omega_n^2) - i\omega Z_n] a_n = (F_a + T(\omega)) \psi_n(0), \quad (8b)$$

$$T(\omega) = -iD_a\omega(z_1 - z_2) + K_a(z_1 - z_2),$$

where z_2 in force $T(\omega)$ is determined by (5) at $r = 0$, applied at the centre of the plate. The quantities ω_n are the angular natural frequencies of the n th flexural mode in a vacuum, accounting for the plate stiffness, h is the thickness of the plate and ρ_s is the density of the plate material (see Appendix A). For the calculation of ω_n , we use the parameters of steel and the thickness, calculated from the plate area, mass and density (Table 1). With amplitudes a_n determined from (8b), we can calculate the displacement z_2 of the flexing plate using (5). Note that (7) was considered for convenience, but the generalized system (8) is not restricted to the case of small wave size of the plate as system (4) was, as it replaced the lumped parameters of the ground with the exact impedances (B5).

It is easy to show that (8b) is identical to the second equation in (4) if the baseplate is rigid (all amplitudes a_n are zero except

a_0 and $z_2(\omega, r) = z_2^{\text{whole}}(\omega)$ in (5)). The eigenfunction $\psi_0(r) = 1/R_0\sqrt{\pi}$ describes the uniform displacement of the plate (see Appendix A) and satisfies the orthogonality conditions (A3). Multiplying both sides of (8b) by $\psi_0(r)$, we obtain

$$[-\rho_s b(\omega^2 - \omega_0^2) - i\omega Z_0] a_0 \psi_0(r) = \frac{F_a + T(\omega)}{\pi R_0^2}. \quad (9)$$

Using $z_2^{\text{whole}} = a_0 \psi_0(r)$ (equation (5)), $S = \pi R_0^2$, $M_2 = \rho_s S b$ and Z_0 determined from (7), in equation (9), we obtain the second equation in system (4). It should be noted here that $\omega_0 = 0$ as there is no rigidity contribution to the uniform displacement of the plate in a vacuum.

System (8) describes the plate displacements in response to a harmonic excitation. In the case of a broadband excitation, it will describe the response to each spectral component of the applied force.

Formally, the determination of the vibroseis response using (8) requires the calculation of the radiation impedance Z_n using the exact equations (B5) for each flexural mode. These calculations are cumbersome and offer little physical insight; a more physically transparent approach exists, which is computationally much simpler. For the small wave size of the plate, it is natural to consider the generalization of the radiation impedance (7) to the n th flexural mode as the sum of

the same terms but with different, generally mode-dependent coefficients, i.e.

$$Z_n(\omega) S = iK_g^n/\omega - i\omega M_g^n + D_g^n(\omega), \quad (10)$$

where K_g^n and M_g^n are the captured rigidity and mass, respectively, and the dashpot constant $D_g^n(\omega)$ is taken as a function of frequency to capture the frequency dependence of the real part of Z_n . This approach is illustrated in Fig. 2, which shows the frequency dependence of the real (top) and imaginary (bottom) parts of the exact impedance, calculated from (B5), for a sandy soil. The values of soil density, wave velocities and plate radius are given in Table 1. The upper horizontal axis in Fig. 2 indicates the baseplate diameter relative to the shear wavelength, to emphasize the trends that will be independent of the soil type. The results of rigorous calculations are denoted by circles. The coefficient $D_g^n(\omega)$, describing the radiation losses, is simply the real part of the rigorous impedance, while the constants K_g^n and M_g^n are obtained by fitting the imaginary part in Fig. 2 at small wave sizes with the polynomial shape of the imaginary part of (10) (dashed lines in Fig. 2, bottom). In order to demonstrate the asymptotic behaviour, the normalized values of impedance $\bar{Z}_n \equiv Z_n/\rho c_1$ are plotted, where ρ is the soil density, and c_1 is the P-wave velocity.

We can draw three conclusions from (10) and Fig. 2. Firstly, at low frequencies, the captured-rigidity term K_g^n/ω dominates

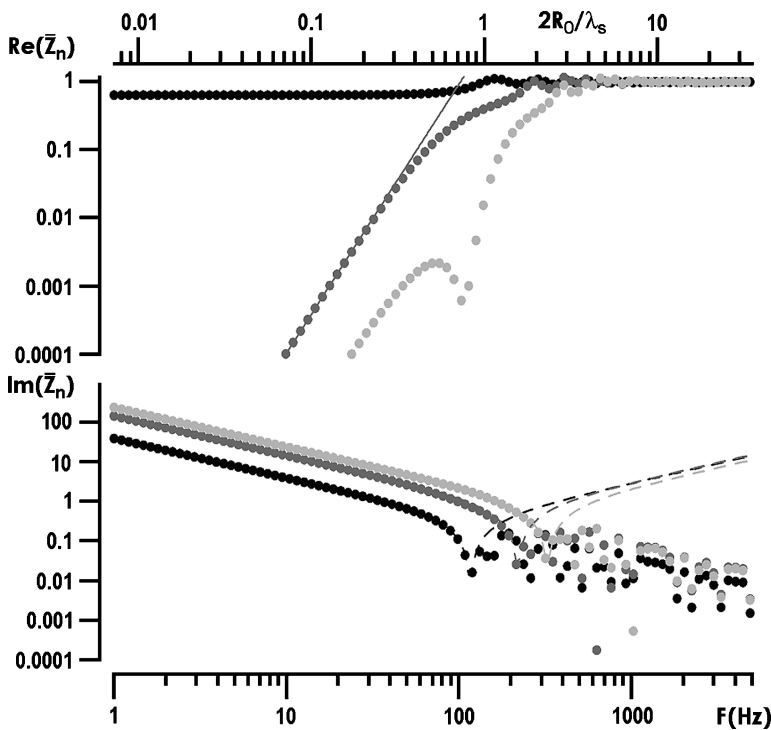


Figure 2 Frequency dependence of the radiation impedance for the baseplate on sandy soil. The impedance Z_n is normalized by ρc_1 : $\bar{Z}_n \equiv Z_n/\rho c_1$. Black symbols correspond to uniform displacement of the plate, dark grey symbols correspond to the first flexural mode, and light grey symbols correspond to the second flexural mode. The solid line at the top of the panel depicts the ω^4 dependence (see Appendix B). The oscillations at high frequencies are due to the Rayleigh pole contribution in (B5).

the imaginary part of (10), which is revealed in the initial ω^{-1} decay of the curves in Fig. 2 (bottom). Since the captured rigidity K_g^n is simply a scaling factor of these curves, we see that it increases slightly with the mode number. Since we also see that $\text{Re}(Z_n)$ at low frequencies is very small (Fig. 2, top), the absolute impedance for the flexural modes at these frequencies is simply the captured-rigidity contribution.

Secondly, (10) clearly provides a good approximation to the imaginary part of the radiation impedance up to a wave size of approximately 1, but it becomes inappropriate above this value where the dashed lines start to diverge from the exact solution. It is thus possible to determine the constants K_g^n and M_g^n from the low-frequency fitting and use them, within these limits of applicability, in the calculations of the impedance, instead of performing tedious calculations with (B5). We use this approach in the following calculations.

Visible oscillations in Z_n at large plate sizes are due to the oscillating character of the radiation of Rayleigh waves as a function of plate size. To understand the physical nature of these oscillations, we consider the case of a uniform pressure applied to the ground. If the plate size is greater than the Rayleigh wavelength, some maxima in the vertical displacement in the Rayleigh wave will be in phase and some will be out of phase with the applied pressure. In the former case the wave is transmitted and in the latter case the wave is damped. The Rayleigh-wave radiation therefore reaches a minimum when maximum compensation occurs. Note that the high-frequency asymptote of the radiation impedance per unit area is $Z_n = \rho c_1$ (an infinite plate), which corresponds to a planar radiated P-wavefront.

Thirdly, the radiation losses $D_g^n(\omega)$ for the flexural modes are significantly lower than their values for the uniform displacement of the plate within the entire seismic frequency band. This fact will be used in the analysis in Appendix B of the low-frequency asymptotic behaviour of the total power radiated by the flexural modes.

System (8) formally consists of an infinite number of equations since the total baseplate displacement is described by the infinite series (5); however, the dimension of the system can be reduced by considering progressively decreasing values of the higher terms in the series. Indeed, we see from (8b) that the decay of the modal amplitudes is inversely proportional to ω_n^2 and Z_n . The resonance frequencies of the flexural vibrations in a vacuum are proportional to the square of the mode number, i.e. $\omega_n^2 \propto n^4$ (Junger and Feit 1986, chapter 7.10). As we have seen in Fig. 2, at small plate sizes the radiation impedance is mainly composed of the captured rigidity, which increases slightly with the mode number. The higher-order terms in se-

ries (5) will therefore decay no slower than $\propto 1/n^4$, providing fast absolute convergence of the series. For this reason, the number of terms in the sum (5) can be limited by a reasonable value N , based on the required accuracy, and system (8) will therefore consist of $N + 2$ equations. In the numerical examples below, the number of modes N was determined so as to provide a relative accuracy in the computed sum of 10^{-3} or better (it was found that $N = 5$ provides a very good approximation of (5)).

Finally, equations (8) provide a formal framework in which to calculate the displacement at an arbitrary point on the baseplate, taking the effect of flexural vibrations into account. However, it may be expected that this effect will not always be significant and in some practical situations may simply be ignored, making detailed analysis unnecessary; hence it would be of practical interest to first evaluate the conditions under which the effect of flexure is overall small.

Examining (1) and (2), it is possible to distinguish between the two causes of the effect of flexure on ground-force measurements. Firstly, this contribution may be significant at the resonance frequencies at which some of the coefficients a_n in (5) become sufficiently large. Secondly, the effect of flexure needs to be accounted for only if the second term in (1) is large relative to the first term; otherwise, the contribution of the baseplate acceleration, whether from the flexural vibrations or vibrations 'as a whole', to the weighted sum (1) will be negligible. This explains why, before describing the results of the full analysis, we next develop a tool for the evaluation of resonance frequencies and then estimate the frequency band in which the value of the second term in (1) is significant.

Resonance frequencies of flexural deformations

Formally, the exact flexural resonance (natural) frequencies $\tilde{\omega}_n$ of the plate on the ground should be determined as the solutions of (8b), by setting the external force (right-hand side) equal to zero and using the rigorous expressions for the impedance Z_n from (B5). However, the rigorous computation of the impedance may not be necessary in the seismic frequency band (small wave size of the plate), where the calculation of the resonance frequencies can be greatly simplified.

Firstly, as we have seen, the impedance values in this case can be accurately approximated by (10). Secondly, the system dissipation does not significantly affect the computation of the resonance frequencies as long as the system's quality factor Q exceeds unity; in this case, the dissipation effect only appears as a small correction, of the order of $1/Q^2$, to the resonance frequencies (Landau and Lifshitz 1976, chapter 25). From the

analysis of the resonance peaks in Fig. 6, the Q -factor is at least 2–3. Therefore, for the calculation of the resonance frequencies (but not in Figs 4–8), (10) can be reduced to its imaginary part, $Z_n(\omega)S \approx iK_g^n/\omega - i\omega M_g^n$.

A further simplification is possible. As can be seen from Fig. 2 (bottom), within the same degree of accuracy, the imaginary parts $\text{Im}(Z_n)$ for the flexural modes and for the uniform displacement of the plate are close to each other. In other words, the resonance frequencies can be computed with the assumption that $K_g^n \approx K_g$ and $M_g^n \approx M_g$, thus yielding the impedance in the form, $Z_n(\omega)S \approx iK_g/\omega - i\omega M_g$. Such an assumption is, for example, made for the elastic-foundation model in mechanical engineering (Timoshenko and Woinowsky-Krieger 1959, chapter 8; Johnson 1985), in which the ground reaction is considered to be independent of the displacement distribution over the plate; the impedance is thus assumed to be independent of the mode number and to be the same as for uniform displacement. In this case, the captured rigidity and mass in (10) are substituted by their values for the uniform displacement (7).

Using these approximations and substituting $Z_n S \approx iK_g/\omega - i\omega M_g$ in (8b) with the right-hand side equal to zero, and with $M_2 = \rho_s h S$, we find a simple solution for the flexural resonance frequencies of the plate on the ground, i.e.

$$\tilde{\omega}_n^2 = \omega_n^2 \frac{M_2}{M_2 + M_g} + \Omega^2,$$

where

$$\Omega^2 = \frac{K_g}{M_2 + M_g},$$

and where, as before, ω_n are the resonance frequencies in vacuum.

Note that the latter formula uses the elastic-foundation model, while a more accurate estimate could be obtained by using the values of K_g^n and M_g^n . The first two flexural resonance frequencies, obtained both ways, are tabulated for muddy soil in Table 2. The muddy soil was chosen because its value of M_g

is a maximum and the value of K_g is a minimum compared with chalky or sandy soils (Table 1). The resonance frequencies are therefore minimized, and we can expect the most pronounced effect of flexure on the baseplate dynamics. As we have seen in Fig. 2, K_g^n increases slightly with the mode number; this is why the more accurate values (the third column in Table 2) slightly exceed the values for the elastic-foundation model (second column). However, the approximations given by the elastic-foundation model are clearly suitable for practical applications.

For the determination of the resonance frequencies of the higher modes, the approximate approach used to calculate the values in Table 2 will, of course, not be applicable, as the plate wave size will not be small or of the order of 1. The frequencies in this case should be calculated using the general approach outlined at the beginning of this subsection. These frequencies will, nevertheless, generally be beyond the seismic band, as those listed in Table 2 for muddy soil represent typical lower boundaries, and will be of little practical interest.

Frequency band where the effect of flexure is significant

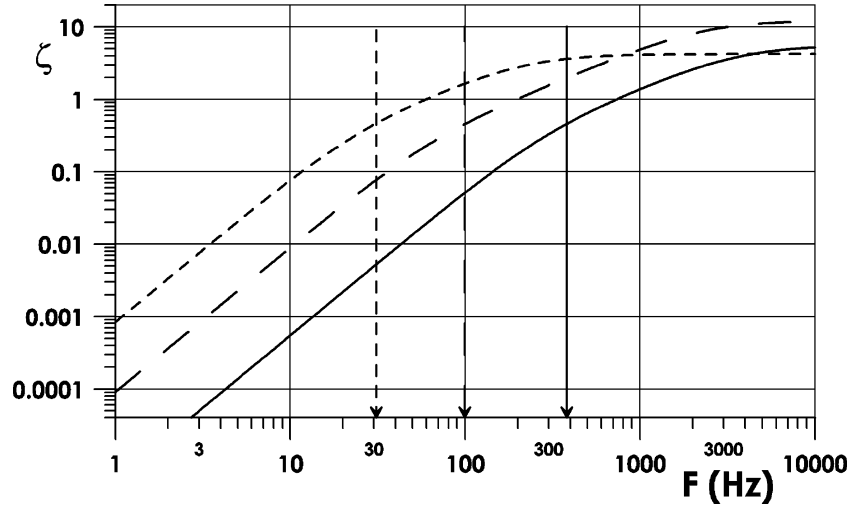
We next evaluate the frequency band in which the contribution from the baseplate acceleration, the second term $M_2 \ddot{z}_2$, to the weighted sum (1) is significant. To make this estimate, we can simply use \ddot{z}_2 obtained for a rigid plate ($\ddot{z}_2 = \ddot{z}_2^{\text{whole}}$), since, if the second term in (1) is comparable to the first term for a rigid plate, the effect of flexure, appearing as a perturbation to \ddot{z}_2 , will certainly not change this relationship.

Figure 3 shows the frequency dependence of the ratio $\zeta = |M_2 \ddot{z}_2 / F_g|$, where F_g is defined by (1). The calculations were made by the standard solution of the original system of linear equations (4). The vertical arrows show the positions of the frequency $\Omega/2\pi$, introduced in the previous subsection. It can be seen that the values of ζ are about 1 at high operating frequencies only (60 Hz for muddy soil and 200 Hz for sand) and above the corresponding $\Omega/2\pi$ in each case. The greatly reduced values of ζ at low frequencies are explained by the growth in the impedance $|K_g/\omega|$ (see equation (7)) and the dominance of K_g over K_a (Table 1). As the flexure affects \ddot{z}_2 as shown in (2), we thus expect that the most significant contribution of flexure will also occur at high frequencies. The compact soils such as chalk are of no interest because $\zeta \approx 1$ at frequencies of 800 Hz, which is outside the vibroseis operating band. As we previously noted, the contribution of flexure could also be significant around the flexural resonance frequencies. Since all the resonance frequencies are higher than $\Omega/2\pi$, as shown in the previous subsection, we conclude that,

Table 2 Resonance frequencies of the displacement of the plate as a whole ($n = 0$) and of the first two flexural modes, for muddy soil

Mode number n	Frequencies determined using elastic-foundation model (Hz)	Frequencies determined using K_g^n and M_g^n (Hz)
0	31	31
1	68	94
2	261	333

Figure 3 The frequency dependence of the contribution of the baseplate displacement ‘as a whole’ to the ground-force signal (1). The solid line corresponds to chalky soil, long dashes correspond to sandy soil, and short dashes correspond to muddy soil. The parameters in (4) are as in Safar (1984) (Table 1).



in all possible scenarios, the contribution of baseplate flexure will be significant only at the high end of the vibroseis operating band.

RESULTS AND DISCUSSION

As we have discovered, the baseplate displacement makes a substantial contribution to the ground-force signal (1) only at sufficiently high frequencies near 100 Hz, and the effect is most pronounced for soft soils such as sand or mud. Consequently, in the following, we focus on sandy and muddy soils. The positions of the reference accelerometer at the centre ($r = 0$) and the edge ($r = R_0$) of the plate will be considered. To estimate the distortion in the correlation function resulting from the contribution of flexural vibrations to the sensor readings, we proceed as follows. We calculate the ground-reaction force (1) without flexure (baseplate moving ‘as a whole’, no $\ddot{z}_2^{\text{flexure}}$ term in equation (2)) as well as with flexure taken into account (finite $\ddot{z}_2^{\text{flexure}}$ term in equation (2)). We call these the ‘ideal’ and the ‘measured’ ground-force signals, respectively. The required terms $\ddot{z}_2^{\text{whole}}$ and $\ddot{z}_2^{\text{flexure}}$ are found from (5), with modal amplitudes a_n ($n > 1$) calculated from (8b) in the latter case. We then correlate these signals with the far-field geophone response and compare the results.

The calculation of the far-field geophone response is based on the equations for the far-field particle velocity developed by Lebedev and Sutin (1996), which are similar to those given by Miller and Pursey (1954). For each spectral component of the sweep-signal, the far-field particle velocity V_z in the vertically propagating P-wave is calculated as (Lebedev and Beresnev 2004, eq.B6)

$$V_z = \frac{ik_1 F \exp(i(k_1 d - \omega t))}{2\pi\rho c_1 d}, \quad (11)$$

where $k_1 = \omega/c_1$, d is the depth to the geophone, and F is the force applied to the ground ($F = -F_g$). This force has been set according to (1) with $\ddot{z}_2 = \ddot{z}_2^{\text{whole}}$, because, as shown in Appendix A, the flexure does not affect the far-field signal. For simplicity, a homogeneous medium is assumed.

Cross-correlation for different accelerometer positions

Figures 4 and 5, respectively, show the results for sandy soil and muddy soil beneath a steel baseplate. The absolute arrival times correspond to a depth of 100 m beneath the baseplate, although the differences we study do not depend on this distance. The sweep frequencies are 15–150 Hz.

We see that the ‘measured’ arrival time can be greater or less than the ‘ideal’ arrival time, depending on where the reference sensor is located with respect to the point of application of the force. The maximum shift is 0.3 ms for sandy soil and 0.6 ms for muddy soil. These shifts seem insignificant, although a value of 0.3 ms is recognizable in vibroseis measurements (Martin and Jack 1990). If arrival-time errors of less than one millisecond are to be avoided, it is necessary to take the effects of baseplate flexure into account.

Physically, the changes in the arrival time are caused by the phase lag in the transfer function defined as the ratio of the ground force F_g , measured by the reference sensor, to the applied force F_a (Fig. 6). As before, the ‘ideal’ ground force is the signal corresponding to the vibrations of the plate without flexure, and the ‘measured’ ground force is the one that includes flexure. It is seen that the phase deviation (Fig. 6, right, curves 1 and 2) may be positive or negative depending on the location of the sensor (the respective cross-correlations are shown in Fig. 5). It is important to note that the

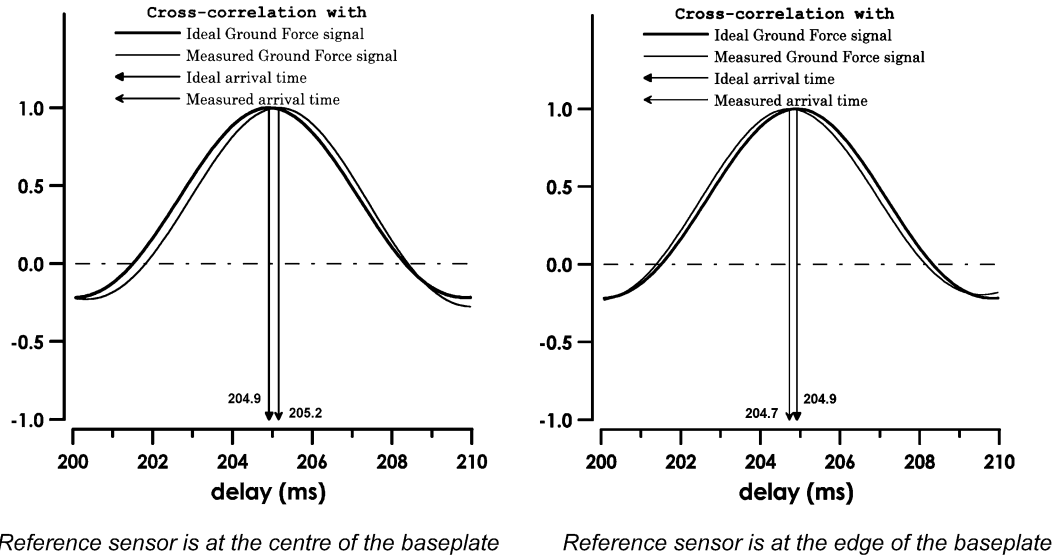


Figure 4 The effect of flexure on arrival time. The numbers at the arrows correspond to arrival times in milliseconds, defined as the abscissae of the peaks. The baseplate is on sandy soil.

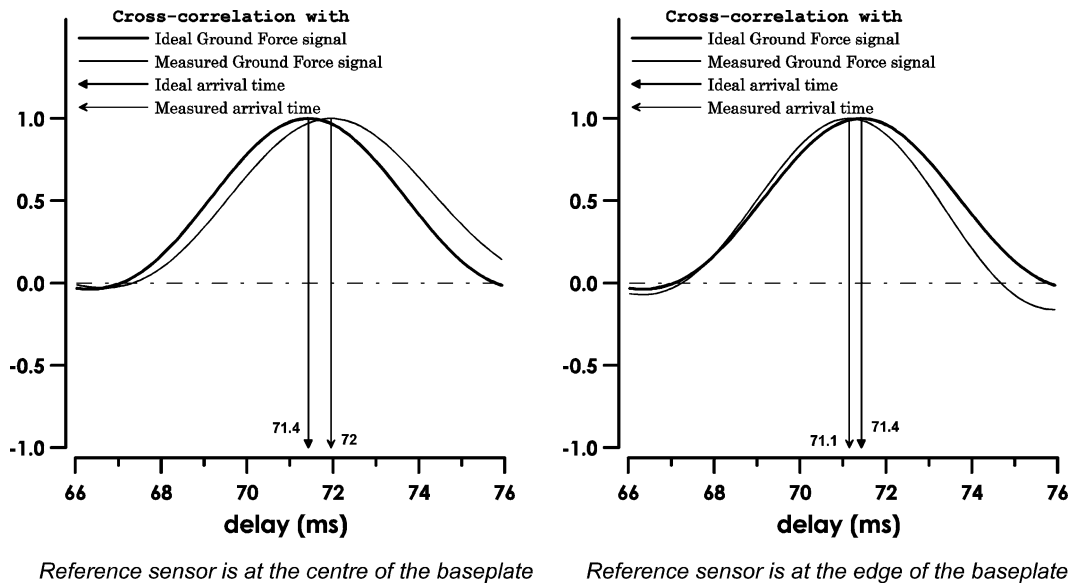


Figure 5 The effect of flexure on arrival time. The numbers at the arrows correspond to arrival times in milliseconds, defined as the abscissae of the peaks. The baseplate is on muddy soil.

deviations occur around the resonance frequencies of the flexural vibrations (dotted arrows). The positive deviations (curve 1) indicate an additional delay in the cross-correlation function, while the negative deviations (curve 2) indicate an earlier arrival.

It follows that we should only be concerned with the effect of flexural vibrations (the position of the reference sensor) on the arrival-time measurements if their resonance frequencies fall within the seismic frequency band. If they are outside

this band, the position of the reference sensor will not realistically matter. It can be shown that the values of the resonance frequencies increase as the ground rigidity increases. A ‘muddy’ soil will therefore represent the worst-case scenario, as its rigidity is the lowest (Table 1). The upper frequency of the sweep signals is typically below 200 Hz. Even for muddy soil, all flexural resonance frequencies except the first one will be above this limit (Table 2); we therefore only need to consider the effect of the first mode.

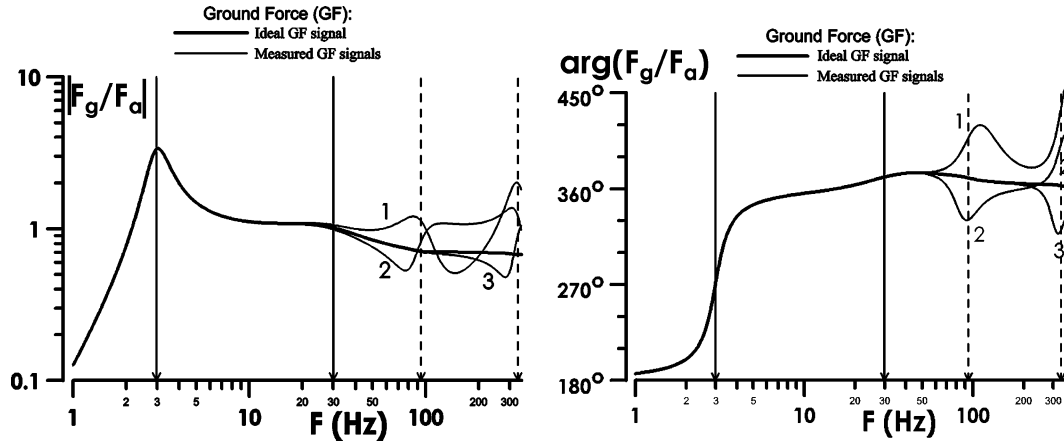


Figure 6 The frequency dependence of the modulus (left) and phase (right) of the transfer function. The calculations were made for muddy soil. The force is applied at the centre of the baseplate. Curves 1 correspond to the reference sensor at the point of excitation ($r = 0$), curves 2 correspond to the sensor located at the edge of the baseplate ($r = R_0$), and curves 3 correspond to the optimum location of the sensor (see text). Solid arrows depict the resonance frequencies of the vibratory system with the rigid baseplate (reaction mass + plate) (Lebedev and Beresnev 2004, fig. 3); dotted arrows correspond to the flexural resonances.

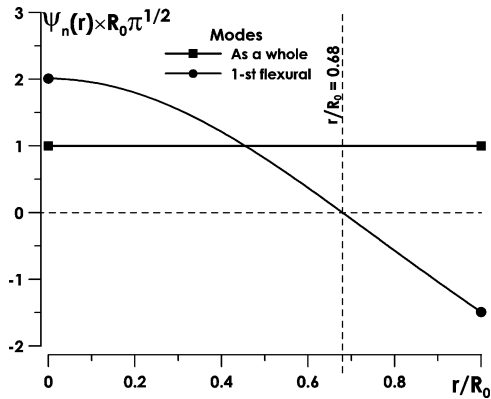


Figure 7 The distribution of displacement along the radius of the baseplate for the first flexural mode. The thin vertical line shows the position of its node.

Reference accelerometer at the nodal line of the first flexural mode

We now check to see if placing the sensor at the node of the first flexural mode will eliminate the error in the arrival time. Figure 7 shows the distribution of displacement in the first flexural mode along the radius of the plate. The node is located at $r \cong 0.68 R_0$. The curves 3 in Fig. 6 correspond to the reference sensor at this nodal position. We see that the additional phase lag is nearly absent below ~ 200 Hz. The cross-correlation between the received and the reference signals for this optimum case is shown in Fig. 8. No shift in the arrival time, caused by the effect of the flexural vibrations, occurs (see Figs 4 and 5). Thus placing the sensor at the node of the first flexural mode eliminates the error.

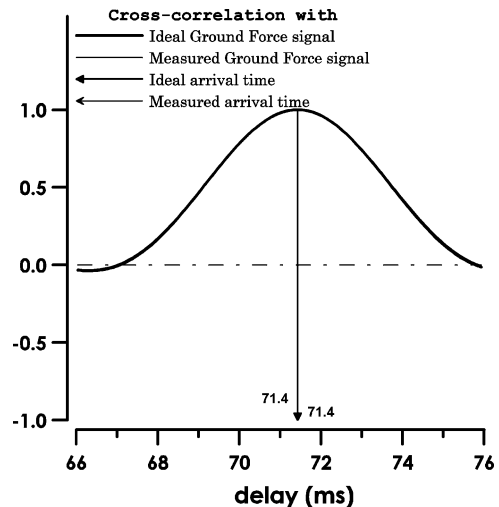


Figure 8 Cross-correlation function for the optimum position of the reference sensor.

In practice, it may be difficult to find the exact nodal line of the flexural mode of the baseplate. A more practical solution to eliminating the effect of the reference-sensor location on the arrival times would be to move the first flexural resonance above the upper frequency of the sweep signal.

SUMMARY AND CONCLUSIONS

We have considered the problem of the effect of flexural deformations on the radiation properties of vibroseis sources. The analysis showed that in most practical applications the

flexural deformations only weakly affect the far-field radiation. We evaluated the frequency band in which the baseplate flexure may contribute considerably to the measured 'weighted-sum' ground-force signal; these frequencies are at the higher end of the vibroseis operating band (around 100 Hz) and are lowest for softer soils.

We calculated the ground-force signal that would be measured by a reference accelerometer placed at different points on the baseplate, with and without flexure being taken into account. The cross-correlation of the far-field signal with these reference signals determines the arrival time of the seismic waves. The effect of moving the accelerometer around the flexing baseplate causes errors in the arrival time of up to 0.6 ms for muddy soil and less for denser soils, relative to the case of a rigid plate. They are therefore rather insignificant. These time shifts are caused by the phase lag in the oscillations of the plate relative to the actuator force, occurring around the resonance frequency of the first flexural mode. Placing a reference sensor on the nodal line of this mode will thus eliminate the traveltime error. However, a more practical solution would be to make the resonant frequencies of the flexural modes higher, moving them beyond the vibroseis operating band, for example, by using plate stiffeners.

Our principal conclusions apply to realistic baseplate shapes in the seismic frequency band. Similar calculations for complex plate geometries at higher frequencies will be much more complicated and physically not as transparent; therefore, they are of little interest for seismic-exploration applications and are beyond the scope of this article.

ACKNOWLEDGEMENTS

This research was supported by WesternGeco. We appreciate the permission of WesternGeco to publish the results. We are indebted to Peter Vermeer and David Hoyle for support and encouragement, and to Peter Vermeer for helpful comments in the course of this work and in the preparation of the manuscript. Thanks are also due to G. Baeten and an anonymous reviewer for helping to improve the clarity of the presentation.

REFERENCES

- Baeten G. and Ziolkowski A. 1990. *The Vibroseis Source*. Elsevier Science Publishing Co.
 Bycroft G.N. 1956. Forced vibrations of a rigid circular plate on a semi-infinite elastic space and on an elastic stratum. *Philosophical Transactions of the Royal Society of London* **A248**, 327–368.

- Gladwell G.M. 1968. The calculation of mechanical impedances relating to an indenter vibrating on the surface of semi-infinite elastic body. *Journal of Sound and Vibration* **8**, 215–228.
 Johnson K.L. 1985. *Contact Mechanics*. Cambridge University Press.
 Junger M.C. and Feit D. 1986. *Sound, Structures and Their Interaction*, 2nd edn. MIT Press, Cambridge, MA.
 Korn G.A. and Korn T.M. 1968. *Mathematical Handbook for Scientists and Engineers*, 2nd edn. McGraw–Hill Book Co.
 Landau L.D. and Lifshitz E.M. 1959. *Theory of Elasticity*. Pergamon Press, Inc.
 Landau L.D. and Lifshitz E.M. 1976. *Mechanics*, 3rd edn. Pergamon Press, Inc.
 Lebedev A.V. and Beresnev I.A. 2004. Nonlinear distortion of signals radiated by vibroseis sources. *Geophysics* **69**, 968–977.
 Lebedev A.V. and Sutin A.M. 1996. Excitation of seismic waves by an underwater sound projector. *Acoustical Physics* **42**, 716–722.
 Lerwill W.E. 1981. The amplitude and phase response of a seismic vibrator. *Geophysical Prospecting* **29**, 503–528.
 Martin J.E. and Jack I.G. 1990. The behaviour of a seismic vibrator using different phase control methods and drive level. *First Break* **8**, 404–414.
 Miller G.F. and Pursey H. 1954. The field and radiation impedance of mechanical radiators on the free surface of a semi-infinite isotropic solid. *Proceedings of the Royal Society (London)* **A223**, 521–541.
 Morse P.M. and Feshbach H. 1953. *Methods of Theoretical Physics*. McGraw–Hill Book Co.
 Robertson I.A. 1966. Forced vertical vibration of a rigid circular disc on a semi-infinite solid. *Proceedings of the Cambridge Philosophical Society: Mathematical Physics* **62**, 547–553.
 Safar M.H. 1984. On the determination of the downgoing P-waves radiated by the vertical seismic vibrator. *Geophysical Prospecting* **32**, 392–405.
 Sallas J.J. 1984. Seismic vibrator control and the downgoing P-wave. *Geophysics* **49**, 732–740.
 Sallas J.J. and Weber R.M. 1982. Comments on 'The amplitude and phase response of a seismic vibrator' by W.E. Lerwill. *Geophysical Prospecting* **30**, 935–938.
 Skudrzyk E. 1968. *Simple and Complex Vibratory Systems*. The Pennsylvania State University Press.
 Timoshenko S. and Woinowsky-Krieger S. 1959. *Theory of Plates and Shells*, 2nd edn. McGraw–Hill Book Co.

APPENDIX A

Radiation efficiency of flexural deformations in the far-field

The set of eigenfunctions (oscillation modes) $\psi_n(r)$ of the plate with free edges forms an orthonormal basis. These functions are obtained as follows. The differential equation for axisymmetric flexural deformations of a thin plate with free boundaries can be written (Skudrzyk 1968, chapter 8) as

$$D\nabla^4 z_2(r, t) + \rho_s b \ddot{z}_2(r, t) = \frac{F(t)\delta(r)}{2\pi r} - \frac{F_g(r, t)}{\pi R_0^2}, \quad (\text{A1})$$

with the boundary conditions (Landau and Lifshitz 1959, p. 51, problem 5)

$$\nabla^3 z_2|_{r=R_0} = 0, \quad \left(\nabla^2 z_2 - \frac{1-\nu}{r} \nabla z_2 \right) \Big|_{r=R_0} = 0, \quad (\text{A2})$$

where r is the distance from the plate centre, R_0 is the plate radius, $D = Eb^3/12(1-\nu^2)$ is the ‘bending’ stiffness, E , ν and ρ_s are the Young modulus, Poisson’s ratio and density, respectively, of the plate material, b is the plate thickness, and $\delta(r)$ is Dirac’s delta-function. The conditions (A2) physically mean that the bending moment and the shear force vanish at the plate boundary. The right-hand side of (A1) is the total force acting on the plate per unit area, which incorporates the force F acting at the plate centre and the ground-reaction force $-F_g$. For an axisymmetric problem, the operators ∇^p are

$$\nabla^4 = \left(\frac{d^2}{dr^2} + \frac{1}{r} \frac{d}{dr} \right)^2, \quad \nabla^3 = \frac{d}{dr} \nabla^2,$$

$$\nabla^2 = \frac{d^2}{dr^2} + \frac{1}{r} \frac{d}{dr} \quad \text{and} \quad \nabla = \frac{d}{dr}.$$

The basis $\psi_n(r)$ satisfies (A2) and (A1) with the right-hand side equal to zero, so that $\nabla^4 \psi_n(r) = \kappa_n^4 \psi_n(r)$, where $\kappa_n^4 = \rho_s b \omega_n^2 / D$ is the flexural wavenumber for the n th mode. The solution of this equation, having no singularity at the plate centre, is $\psi_n(r) = A_n J_0(\kappa_n r) + B_n I_0(\kappa_n r)$, where $J_0(x)$ is the Bessel function of zero order and $I_0(x)$ is the modified Bessel function of zero order (Skudrzyk 1968, eq.8.31). The values of $\kappa_n R_0$ and the ratio B_n/A_n are determined from the boundary conditions (A2). Specifically, the first equation in (A2) allows us to exclude B_n , i.e.

$$\psi_n(r) = A_n \left(J_0(\kappa_n r) - \frac{J_1(\kappa_n R_0)}{I_1(\kappa_n R_0)} I_0(\kappa_n r) \right)$$

for $n > 0$, where $J_1(x)$ and $I_1(x)$ are the corresponding Bessel functions of the first order. This expression is then used in the second equation (A2) to find the values of $\kappa_n R_0$, which will depend on the material of the plate through Poisson’s ratio ν . The resulting transcendental equation for $\kappa_n R_0$ is solved numerically (parameters as in Table 1) to provide the roots $\kappa_1 R_0 = 3.0005$, $\kappa_2 R_0 = 6.2003$, $\kappa_3 R_0 = 9.3675$, \dots , $\kappa_n R_0 \cong \pi n$. Finally, the value of A_n (amplitude) is found from the orthogonality condition,

$$2\pi R_0^2 \int_0^1 \psi_m(x) \psi_n(x) x dx = \delta_{nm}, \quad x = r/R_0. \quad (\text{A3})$$

where δ_{nm} is the Kronecker delta.

The natural frequencies in (8b) are $\omega_n^2 = D\kappa_n^4/\rho_s b$. The uniform displacement of the plate (displacement ‘as a whole’) corresponds to $\psi_0(r) = 1/R_0 \sqrt{\pi}$, which clearly satisfies (A2)

and (A1) with the right-hand side equal to zero. The flexural modes with $n = 1$ are orthogonal to the uniform displacements ($\delta_{0n} = 0$). As a result, the integral over the plate area is

$$2\pi \int_0^{R_0} \psi_n(r) r dr = 0, \quad n > 0. \quad (\text{A4})$$

If the plate size is small relative to the radiated wavelengths, $k_{1,2} R_0 \ll 1$, the ground-reaction pressure for each flexural mode is

$$-P_n = \frac{K_g^n a_n}{\pi R_0^2} \psi_n(r), \quad (\text{A5})$$

where $k_{1,2} = \omega/c_{1,2}$, ω is the angular frequency, and c_1 , c_2 are the P- and S-wave velocities, respectively. The value of K_g^n in (A5) is the captured rigidity, which is possible to determine using the approach described by (10).

Because of (A4) and (A5), the total ground force (the pressure integrated over the plate area) produced by flexure is zero. To calculate the far-field radiation from the flexural mode, it is helpful to distinguish between the areas with positive and negative pressures separated by the nodal lines (zeros of $\psi_n(r)$), whose contributions to the far field should be summed. We consider, for simplicity, the far-field radiation from the first flexural mode, which has only one nodal line located at the radius $r_1 \cong 0.68 R_0$ (Fig. 7). In the case of small plate size, the field radiated by the distribution of positive and negative pressures can be represented as the sum of the fields from two equivalent circular sources of opposite sign, one with radius r_1 and the other with radius R_0 , which would provide the same zero pressure integral over the plate area. The pressure is constant over each of the circular sources (Fig. 9). The problem of the calculation of the far-field radiation from a flexural mode is thus reduced to the calculation of the sum of the fields from two piston sources with uniform pressure.

The far-field displacement for a uniform-pressure circular piston is proportional to the ground force multiplied by the factor

$$f(kR \sin \theta) = \frac{2J_1(kR \sin \theta)}{kR \sin \theta},$$

where $k = \omega/c$, c is the phase velocity of P-, S- or Rayleigh waves, R is the radius of the piston, and θ is the angle measured clockwise from the down direction (Junger and Feit 1986, chapter 5, eq.5.10; Lebedev and Beresnev 2004, appendix B).

Assuming two equivalent piston sources, in which the negative pressure is constant over the piston $r = r_1$ and the positive pressure is constant over the piston $r = R_0$ (Fig. 9), the far-field displacement U_p in the P-wave due to flexure is given by

$$U_p \propto \frac{2J_1(k_1 R_0 \sin \theta)}{k_1 R_0 \sin \theta} - \frac{2J_1(k_1 r_1 \sin \theta)}{k_1 r_1 \sin \theta}. \quad (\text{A6})$$

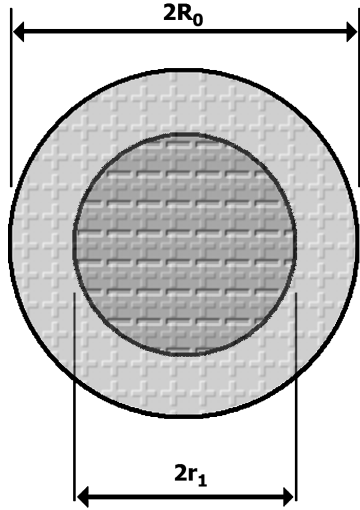


Figure 9 Two equivalent sources for the example considered (radiation from the first flexural mode).

As long as $k_1 R_0 \ll 1$, (A6) can be re-written using a low-frequency ($x \ll 1$) asymptote of the Bessel function,

$$J_1(x) \cong \frac{x}{2} \left(1 - \frac{x^2}{8}\right)$$

(Korn and Korn 1968). As a result, the far-field displacement due to flexure is

$$U_p \propto \frac{k_1^2 R_0^2 \sin^2 \theta}{8} \left(1 - \frac{r_1^2}{R_0^2}\right).$$

The contribution of the flexure to the far field is thus proportional to the far field produced by the displacement as a whole, multiplied by the factor $k_1^2 R_0^2$. Similar equations with $k_1^2 R_0^2$ terms can be obtained for the higher flexural modes. Clearly, U_p is zero for the downgoing ($\theta = 0$) P-wave (the case of total cancellation of the positive and negative contributions emitted from the different parts of the plate). Assuming $k_1 R_0 \ll 1$, the P-wave radiation due to flexure is also negligible relative to the radiation from a rigid plate for any non-zero angle. In Appendix B, we show that the flexural vibrations give a negligible contribution to the total radiated power.

APPENDIX B

Radiation impedance and total radiated power for flexural modes

The standard definition of the modal radiation impedance per unit area is the ratio of the modal pressure to the modal veloc-

ity normal to the vibrating structure (e.g. Junger and Feit 1986, eq.2.26). Strictly speaking, the impedance calculation should involve setting a given modal displacement distribution over the plate, finding the resulting pressure, and taking their ratio (a ‘displacement-to-pressure’ approach). However, the level of complexity in such calculations increases dramatically because Fredholm integral equations must be solved (Robertson 1966). On the other hand, it is known that the values of the radiation impedance for a uniform pressure distribution (Miller and Pursey 1954) and uniform displacement distribution (Bycroft 1956) are only slightly different. For example, it can be shown using expressions given by Johnson (1985, chapter 3) that the captured rigidity for the uniform displacement is less than 10% greater than its value obtained for uniform pressure, and we know that the captured rigidity is a good approximation of the absolute impedance in the seismic frequency band (see discussion of Fig. 2). The same conclusion will therefore hold for the modal displacements. Because of this equivalence, a mathematically simpler ‘pressure-to-displacement’ approach is widely used (Gladwell 1968). We follow this approach in our calculations of the rigorous impedance, by calculating the modal displacement distribution resulting from given modal pressure and taking the ratio, as illustrated below.

Using the Fourier–Hankel integral representation of the radiated displacement field (Miller and Pursey 1954, eq.125; Lebedev and Sutin 1996), we can write the expression for the vertical component of the surface displacement produced by a point force as

$$z_2(r) = \frac{i\omega F}{2\pi\rho c_2^3} \int_0^\infty \frac{\tau\sqrt{\gamma^2 - \tau^2}}{D(\tau)} J_0(k_2 r \tau) d\tau, \tag{B1}$$

where ρ is the density of the soil beneath the baseplate, $\gamma = c_2/c_1$, c_1 and c_2 are the P- and S-wave velocities in the soil, $k_2 = \omega/c_2$, F is the force applied to the ground, and $D(\tau) = (1 - 2\tau^2)^2 - 4\tau^2\sqrt{(\tau^2 - \gamma^2)(\tau^2 - 1)}$ is the Rayleigh denominator.

To calculate the surface displacement produced by a force distribution over the plate due to the n th mode, $F_g^n(r) = f_n \psi_n(r)$, where f_n is the amplitude factor, this distribution must be convolved with the Green’s function (B1). This results in the displacement,

$$z_2(r) = \frac{i\omega f_n}{2\pi\rho c_2^3 S} \int_0^\infty \frac{\tau\sqrt{\gamma^2 - \tau^2}}{D(\tau)} \hat{\psi}_n(\tau) J_0(k_2 r \tau) d\tau, \tag{B2}$$

where $\hat{\psi}_n(\tau) = 2\pi \int_0^{R_0} \psi_n(r) r J_0(k_2 r \tau) dr$ is the Fourier–Hankel image of the modal function $\psi_n(r)$ and S is the plate area.

The amplitude of the modal displacement in (5) is equal to the integral

$$a_n = 2\pi \int_0^{R_0} z_2(r) r \psi_n(r) dr, \quad (\text{B3})$$

which can be directly verified by substituting (5) in (B3) and using the orthogonality of the functions $\psi_n(r)$. Using $z_2(r)$ from (B2) in (B3) then gives

$$a_n = \frac{i\omega f_n}{2\pi \rho c_2^3 S} \int_0^\infty \frac{\tau \sqrt{\gamma^2 - \tau^2}}{D(\tau)} \hat{\psi}_n^2(\tau) d\tau. \quad (\text{B4})$$

The radiation impedance per unit area therefore is

$$Z_n \equiv \frac{f_n}{-i\omega a_n S} = \frac{2\pi \rho c_2}{k_2^2 \int_0^\infty \frac{\tau \sqrt{\gamma^2 - \tau^2}}{D(\tau)} \hat{\psi}_n^2(\tau) d\tau}. \quad (\text{B5})$$

In the case of an inflexible baseplate ($n = 0$), the eigenfunction is $\psi_0(r) = 1/R_0\sqrt{\pi}$. Its Fourier–Hankel image is $\hat{\psi}_0(\tau) = R_0 \Xi(\tau)$, where $\Xi(\tau) = 2J_1(k_2 R_0 \tau)/k_2 R_0 \tau$, and (B5) reduces to the corresponding impedance obtained earlier (Lebedev and Beresnev 2004, eq.C3).

Using the impedance (B5), the total radiated power for the n th harmonic mode can be calculated as the integral of power flux over the baseplate area (Junger and Feit 1986). Omitting simple manipulations, we obtain

$$W_n^{\text{total}} = \text{Re} \left(\frac{|f_n|^2}{2Z_n S^2} \right). \quad (\text{B6})$$

To understand the total power radiated in the flexural modes, it is useful to consider the high- and low-frequency asymptotic behaviour of (B6).

As seen from Fig. 2, at high frequencies ($k_2 R_0 \gg 1$), the real part of the radiation impedance dominates over the imaginary part, and the absolute impedance approaches ρc_1 (see Junger and Feit 1986, figs 5.6, 6.3 and 6.5). Equation (B6) in this case coincides with the equation for the radiation power in P-waves

(e.g. Lebedev and Beresnev 2004, eq.A6). We conclude that, at high frequencies, the flexural modes radiate only P-waves.

At low frequencies, the radiation impedance can be approximated by expression (10). Substituting (10) in (B6) and assuming $\omega^2 \ll K_g^n/M_g^n$, we obtain an asymptotic expression,

$$W_n^{\text{total}} \cong \frac{|f_n|^2 \omega^2}{2(K_g^n)^2 S} D_g^n. \quad (\text{B7})$$

Calculations show (see discussion on how to estimate K_g^n and M_g^n using the elastic–foundation model in subsection ‘Resonance frequencies of flexural deformations’) that the condition $\omega^2 \ll K_g^n/M_g^n$ is satisfied in the frequency domain of interest for most hard surfaces, but may be violated at frequencies above approximately 40 Hz for softer soils such as mud. Within these limits, (B7) can be used to estimate W_n^{total} , thus providing a transparent physical view of the factors controlling the radiated power.

As (B7) shows, because K_g^n is only slightly dependent on the mode number (see discussion on Fig. 2), in order to understand the relationship between the power radiated in different modes for small plate sizes, we only need to compare the values of $D_g^n(\omega) = \text{Re}(Z_n)$, plotted in Fig. 2 (top). For $n = 0$ (displacement as a whole), the value of $\text{Re}(Z_n)$ is nearly constant. As a result, as (B7) shows, the total radiated power is proportional to the square of the frequency, which is a well-known result (Miller and Pursey 1954; Lebedev and Sutin 1996). For the flexural deformations, however, the value of $\text{Re}(Z_n)$ for small plate sizes is much smaller and is scaled as the fourth power of frequency (Fig. 2, top, solid line), which results in $W_n^{\text{total}}(\omega)$ in (B7) becoming proportional to ω^6 . Because of this trend, the total power radiated by the flexural modes remains negligibly small compared with that from the rigid plate at small plate sizes, just as their contribution to the far field is negligible (Appendix A).